Supporting Information

A polarization-actuated plasmonic circulator

Tzu-Yu Chen,† Dhruv Tyagi, † Yun-Chorng Chang,≠ and Chen-Bin Huang†,≠,*

† Institute of Photonics Technologies, National Tsing Hua University, Hsinchu 30013, Taiwan

≠ Research Center for Applied Science, Academia Sinica, Nangang Taipei 11529, Taiwan

*robin@ee.nthu.edu.tw

This article provides supplementary information to the main text of the manuscript. We provide details of the symmetric and anti-symmetric modal profile of the plasmonic two-wire transmission-line (TWTL), TWTL parameter considerations, and antenna design procedures.

1. SPP field profiles for symmetric and anti-symmetric modes

Our numerical simulations are performed using FDTD Solutions by Lumerical Incorporated. For a plasmonic two-wire transmission-line (TWTL), two orthogonal propagation modes exist, namely the symmetric and the anti-symmetric modes. Their modal field and charge density profiles are provided in Figure S1.

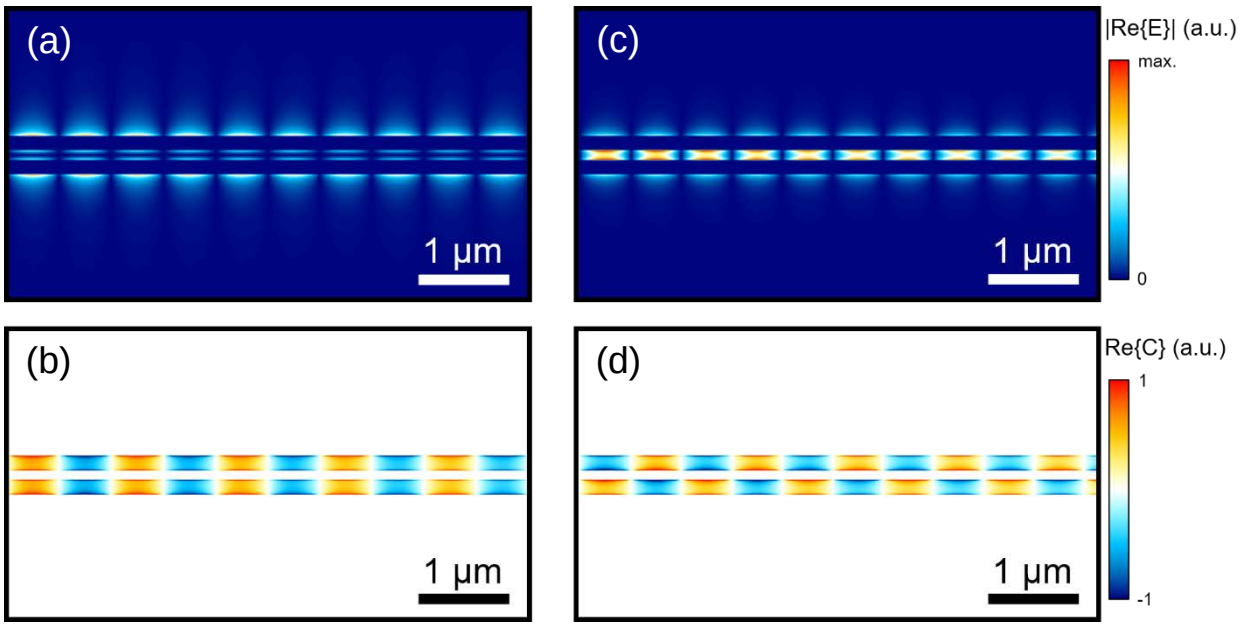

Figure S1. FDTD profiles for: (a) electric field and (b) charge density of the symmetric mode, (c) electric field and (d) charge density of the anti-symmetric mode.

In Figure S1, one finds that for the symmetric mode, the electric fields (Figure S1(a)) are guided along the outer edges of the nanowires, and the charge distritbutions on the two wire are identical (Figure S1(b)). On the other hand, the anti-symmetric mode has a tightly confined electric fields within the central gap (Figure S1(c)), while having opposite signs of charge density on the two wires. Experimentally, the two modes can be independently excited, depending on the orientation of the a linearly-polarized laser Gaussian beam. The symmetric mode is excited when the linear poalrization is along the wire direction, whiel the anti-symmetric mode is excited when the laser is polarized perpendicular to the wires.

2. Performance degradation analysis

The symmetric and anti-symmetric modes have different in-coupling responses (efficiency as well as phase) from a free-spaced laser Gaussian beam into the TWTL. The ideal operation of our plasmonic circulator requires effective destructive (constructive) interference of these two independent modes on one of the two nanowires. To achieve this, four factors are to be satisfied: (I) the fields generated for both the modes should have the equal amplitude; (II) the relative phase delay between the two modes should be either 0 or π; (III) the effective refractive indices for both modes should be similar; and (IV) the loss coefficients for both modes should be comparable. The ideal field profile under complete destructive (constructive) interference is provided in Figure S2.

One could find when all four factors are satisfied, the resulting SPP field perfectly guided only by the bottom nanowire. In the following subsection, the effect of each degradation factor is addressed individually.

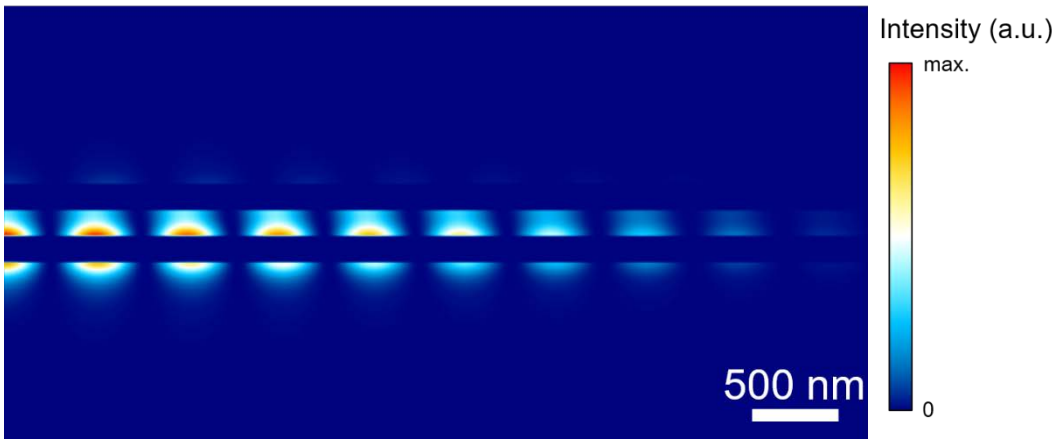

Figure S2. Ideal field profile under complete destructive interference between the two modes.

2.1. Unequal amplitude

When the symmetric and anti-symmetric modes coexist but the their modal fields are having unequal amplitudes, perfect destructive interference on one of the nanowire cannot be satisfied. Figure S3 shows the situation when the relative electric field amplitude ratio for symmetric to anti-symmetric modes is taken to be 2. Weak SPP signal on the top nanowire can be clearly observed, thus hindering the circulator directionality.

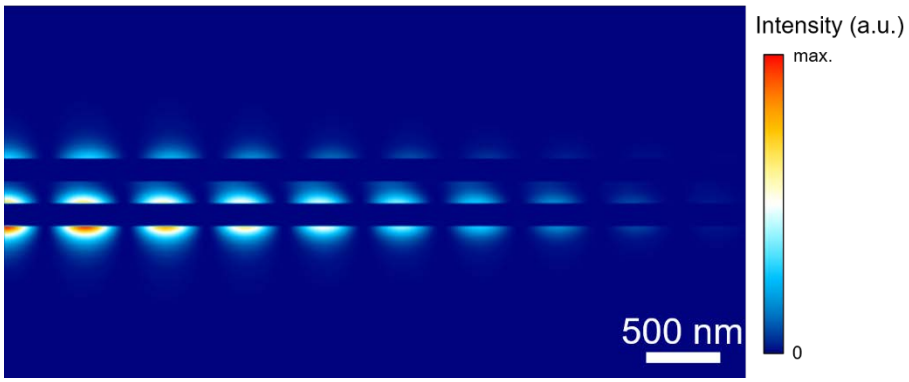

Figure S3. Simulation results of SPP intensity for amplitude ratio of 2:1 between the symmetric and anti-symmetric modes.

2.2. Unequal phase

Similar to the requirement on equalized amplitude, maintaining a proper phase delay between the two modes is equally critical. The phase delay should ideally be either 0 or π. For conceptual understanding and comparisons, Figure S4 shows the FDTD result where the phase difference between the two modes is set to $\pi/2$. The SPP intensities of the two nanowires have almost equal values, which undermines the cirulator operation.

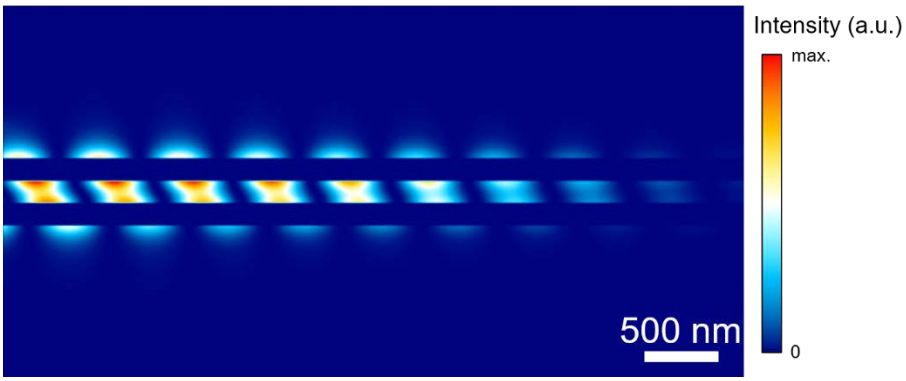

Figure S4. SPP intensity with phase difference of $\pi/2$ between the symmetric and anti-symmetric modes.

2.3. Unequal modal index

In a plamonic TWTL, the symmetric mode and anti-symmetric mode would nevertheless have distinct modal indices. The different real part of the complex propagation constant means the two modes have different effective wavelengths as well as propagation velocities. When the two modes coexist in the TWTL, one would therefore anticipate periodical oscillations of intensity as the SPPs propagate on the TWTL. Figure S5 shows the FDTD simulation assuming a modal index difference of 0.11 (modal indices of 1.51 for symmetric mode and 1.62 for anti-symmetric mode). For such index difference, the intensity oscillation period is 14.1 μm. In our fabricated device, the TWTL geometries were designed to minimize the modal index difference down to 0.02, thus extending the oscillation period to 71 μm. At the same time, we kept the TWTL region length to only 0.4 μm, well within the oscillation period to avoid such undermining periodical energy transfer.

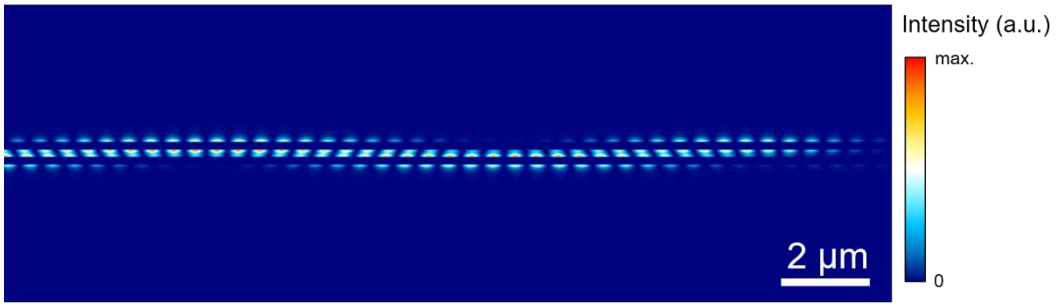

Figure S5. FDTD result for a refractive index difference of 0.11 between the two modes.

2.4. Unequal decay length

If the two modes have different decay lengths (the imaginary part of the complex propagation constants), the ability to maintain SPP guided by only a single nanowire (the degree of destructive interference) would also degrade as a function of propagation length down the TWTL. Figure S6 shows the SPP intensity by assuming loss coefficients of 1.401 (1/μm) and 1.010 (1/μm) for symmetric mode and anti-symmetric mode, respectively. Evidently, initially the SPPs are only confined by the top nanowire. However, as the SPP propagates further to the right (~5 μm), only symmetric mode remains while the anti-symmetric mode field completely decayed. After this propagation length, circulation ceases to function. In our practical device, the TWTL geometries were designed to support loss coefficients of 0.113 (1/μm) and 0.233 (1/μm) for symmetric mode and anti-symmetric mode, respectively. The decay length difference is therefore 8.333 (μm), well beyond the designed TWTL region length of 0.4 μm.

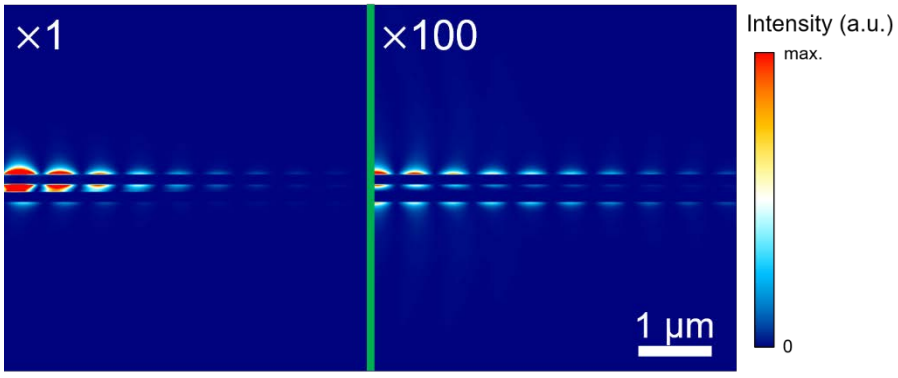

Figure S6. FDTD result for a decay length difference of 0.390 (1/μm) between the two modes.

3. Design of the link antenna

The TWTLs can be used for both exciting SPPs by incident electromagnetic radiation, as well as coupling the SPPs into far-field radiation. This reversibility of radiation coupling from far-field to near-field SPPs and vice-versa is employed for the functioning of the circulator. By irradiating the TWTL by electric field parallel to the nanowires (hereon referred to as the TM polarization), the symmetric mode of SPPs are excited as depicted in Figure S7(a). By irradiating TWTL with electric field perpendicular to the nanowires (TE polarization), the anti-symmetric mode of SPPs is excited as shown in Figure S7(b). The same structure can be used to couple propagating SPPs into far-field radiation. The polarization of the radiated far-field signal is dependent on the mode propagating through TWTL. As shown in Figure S7(c), TM polarized light is radiated when symmetric SPP mode is propagating through the TWTL, and TE polarized light is radiated when anti-symmetric SPP mode is propagating through the TWTL as shown in Figure S7(d). Thus, by controlling the SPP modes in the wire, the polarization state of the radiated signal can be controlled.

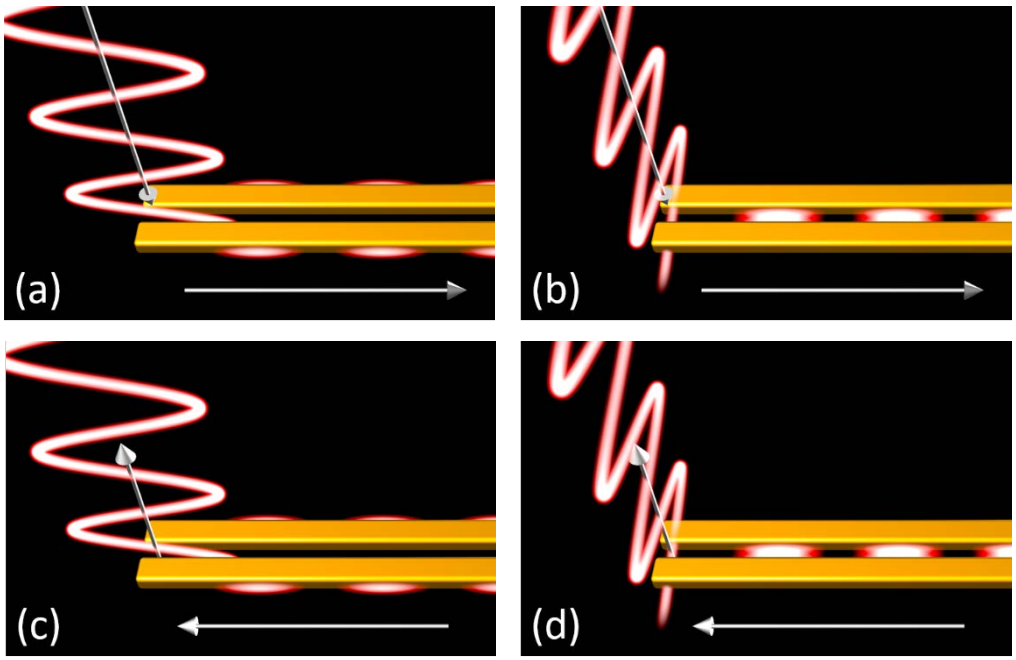

Figure S7. (a) Incident polarization parallel to the nanowires excites the symmetric mode. (b) Incident polarization perpendicular to the nanowires excites the anti-symmetric mode. (c) A guided symmetric mode on the TWTL radiates electric field polarized parallel to the nanowires at the antenna. (d) A guided anti-symmetric mode on the TWTL radiates electric field polarized perpendicular to the nanowires at the antenna.

We need a resonant link antenna to couple TE polarized light to anti-symmetric SPP mode. Figure S8 shows the structure of the link antenna and cross sectional image of TWTL. To satisfy the resonance conditions at the operational wavelength, the optimization of parameters such as the length of the link antenna l_l, width of the wire w, and gap w_g between the two wires is warranted. The effective coupling cross section also depends on the width w_l of the link antenna as well.

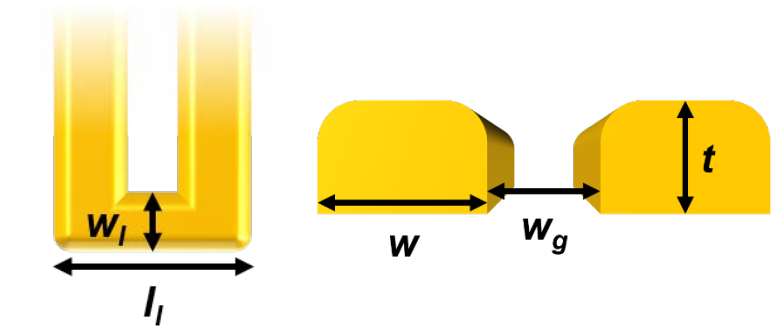

Figure S8. Parameters for link antenna port structure.

We fixed the thickness t to be 60 nm in our simulations and experiments. Although the thickness plays a part in defining the resonance condition for the structure, the effect of t is comparatively less as compared to other parameters such as l_l, thus having more flexibility for our choice of selection. The length l_l being the most important parameter to define the operational wavelength of the circulator needs to be optimized. Varying l_l also generates a phase delay between the symmetric and anti-symmetric mode. During simulations, we optimized w_g to be 100 nm and w to be 160 nm and plotted the amplitude ratio for TM and TE polarization for the radiating far-fields with respect to l_l as shown in Figure S9(a). The ratio reached the optimum value of 1:1 for l_l = 420 nm. Figure S9(b) shows the phase delay with respect to l_l. We can see that for l_l = 420 nm and w_l =70 nm, the phase delay is near 0 resulting in polarization of 45^o of the radiating far-field signal.

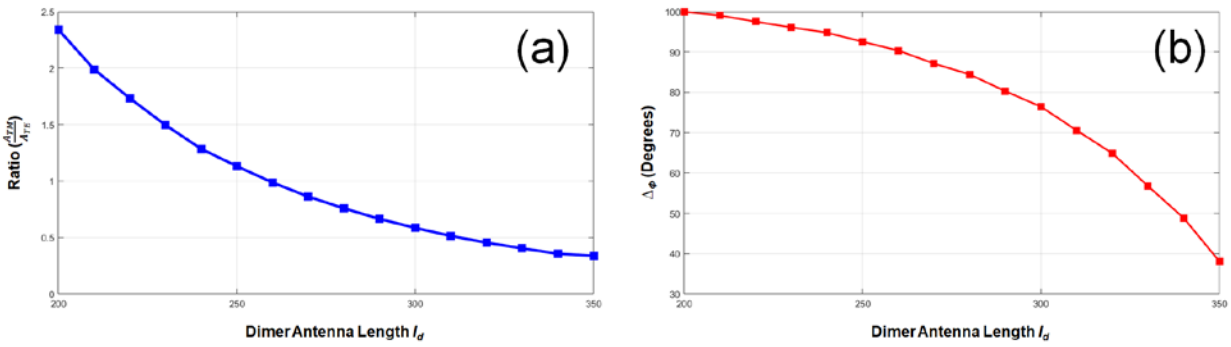

Figure S9. (a) Amplitude ratio of TM to TE component of the output light. (b) Phase difference between TM and TE component.

Once the design parameters are optimized we performed FDTD calculations for ±45° polarization of the excitation source. The field magnitude profile is shown in Figure S10(a) for 45° and Figure S10(b) for −45°. It's clear from these simulation results that the circulator is highly efficient in directing light for these particular polarizations.

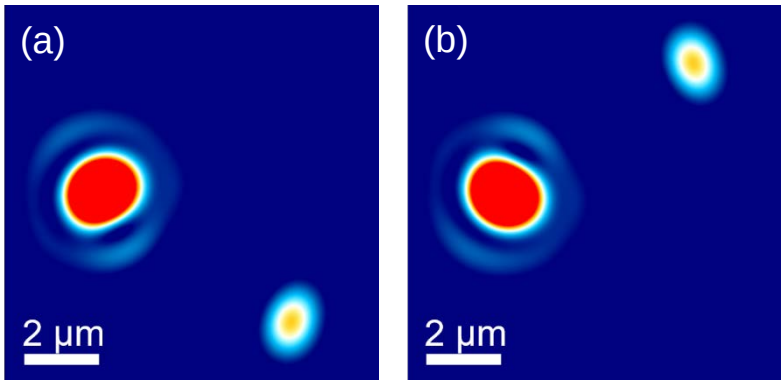

Figure S10. Electric field intensity for the SPP fields when the incident light is (a) 45° and (b) −45° linearly polarized.

4. Design of dimer antenna for spin-actuated circulator

Structural parameters such as w and w_g are optimized for the excitation of symmetric and anti-symmetric SPP modes. Thus, for exciting the circulator by circular polarizations, we are required to discard the link antenna since for the same l_l we cannot have an optimized intensity ratio and phase delay required. If we modify l_l for operation under circular polarization, the parameters for mode excitation will be inconsistent with the TWTL optimization. This is resolved by employing a dimer antenna instead of a link antenna since it provides freedom for dimensional selection to

achieve necessary intensity ratios and phase delays between symmetric and anti-symmetric modes without influencing the TWTL optimized parameters.

Figure S11 shows the structure of the dimer antenna and cross sectional image of TWTL. Here, w_d is the width of the antenna, and l_d is the length of one arm of the dimer antenna. An optimized dimer antenna also resonates for TE polarized excitation source resulting in coupling the incident radiation to anti-symmetric SPP mode. The resonance conditions are dependent on l_d which provides the excitation amplitude and phase for the anti-symmetric SPP mode. By optimizing parameters l_d, w and w_d we can get the perfect intensity ratios and phase conditions for coupling incident symmetric and anti-symmetric polarization to the desired mode excitation. The w_g and t have a very small effect on the resonance and phase conditions and are fixed to be 120 nm and 60 nm respectively, following the dimensions for TWTL with link antenna.

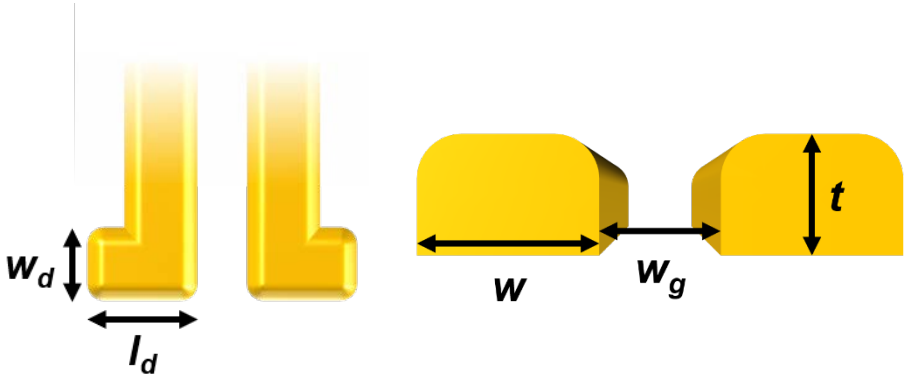

Figure S11. Design parameters for the dimer antenna.

We selected length l_d so that the phase difference between the two modal fields reaches a value of $\pi/2$. Thus, by optimizing w and w_d, the amplitudes for these components can be controlled to have equal values resulting in circular polarization for the emited light. The simulation results are shown in Figure S12(a) with parameter w fixed at 140 nm and w_d at 160 nm. The corresponding polarization state of the output light signal for different l_d is shown. We can clearly see that over the sweep l_d=260 nm gives a near-perfect circular polarization.

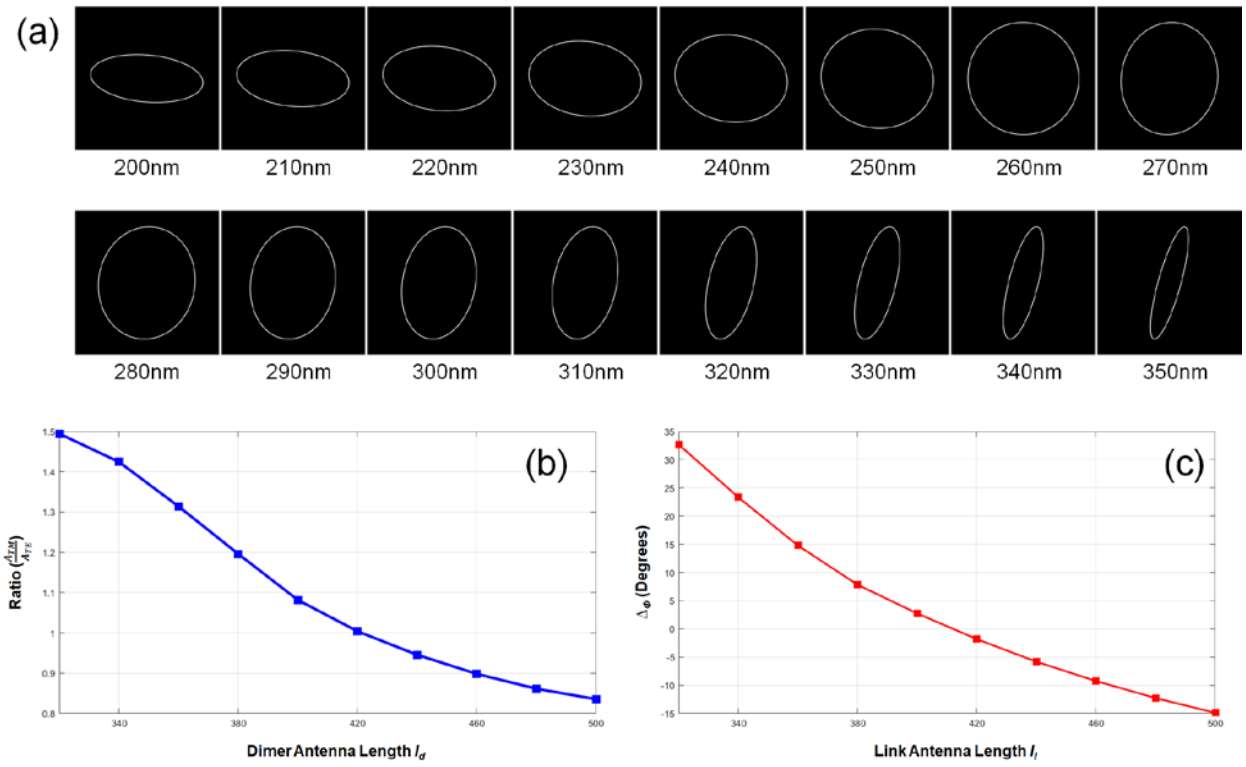

Figure S12. (a) Polarization state of output light with different dimer antenna length. (b) Amplitude ratio of TM to TE component of the output light. (c) Phase difference between TM and TE component.

We we can see in Figure S12(b) that for $\boldsymbol{l_d}$ =260 nm, the amplitude ratio for the two modes is optimum at 1:1. The phase difference with respect to $\boldsymbol{l_d}$ is plotted in Figure S12(c), and for for $\boldsymbol{l_d}$ =260 nm the phase difference is $\pi/2$. Once the design parameters are optimized, we performed FDTD calculations for both right-hand circular polarized and left-hand circular polarized excitation source as shown in Figure S13(a) and Figure S13(b), respectively. It's clear from these simulation results that the circulator is highly efficient in directing light for the circular polarizations as well.

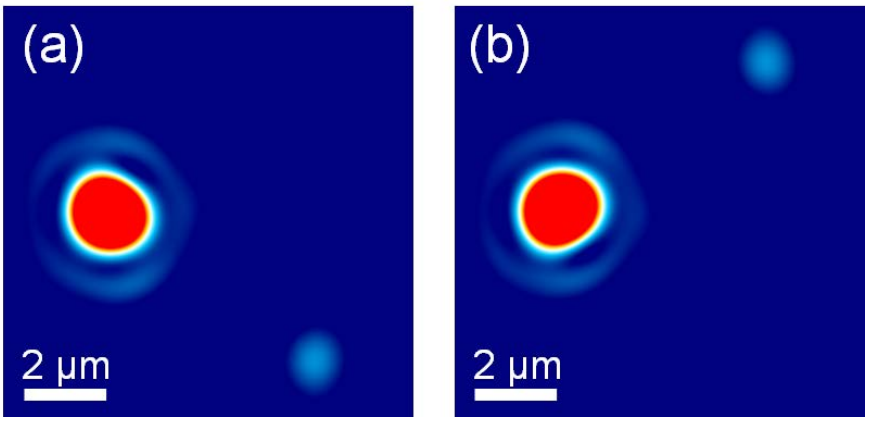

Figure S13. Electric field intensity for the SPP fields when the incident light is (a) RHCP (b) LHCP light source input.

5. Polarization analysis of the scattered output beam

The proposed structure has been designed to operate as a circulator for both linear and circular polarizations. When the circulator is excited using 45 degrees linearly polarized light at port A as can be seen in Figure S14(a), the SPPs propagate through the single wire connecting port A to port B. The SPPs are thereafter scattered to the far-field from port B with a 90 degrees polarization shift. Thus the output light has -45 degrees polarization orientation. It is worth mentioning that the coordinate system considered here is local to each port, where the long axes of link/dimer antennas are perpendicular to the x-axis. The proposed circulator is capable to route SPPs in both clockwise and counter-clockwise fashion. Therefore, the circulator is excited using -45 degrees linearly polarized light at port A, the SPPs propagate through the single wire connecting port A to port C. The SPPs are thereafter scattered to far-field from port C with a 90 degrees polarization shift leading to 45 degrees polarization orientation of the output beam. The structure follows the same working principle for all ports for any number of ports designed under this rule. Figure S14(b) shows the functioning of the circulator when port B is excited by 45 degrees incident polarization.

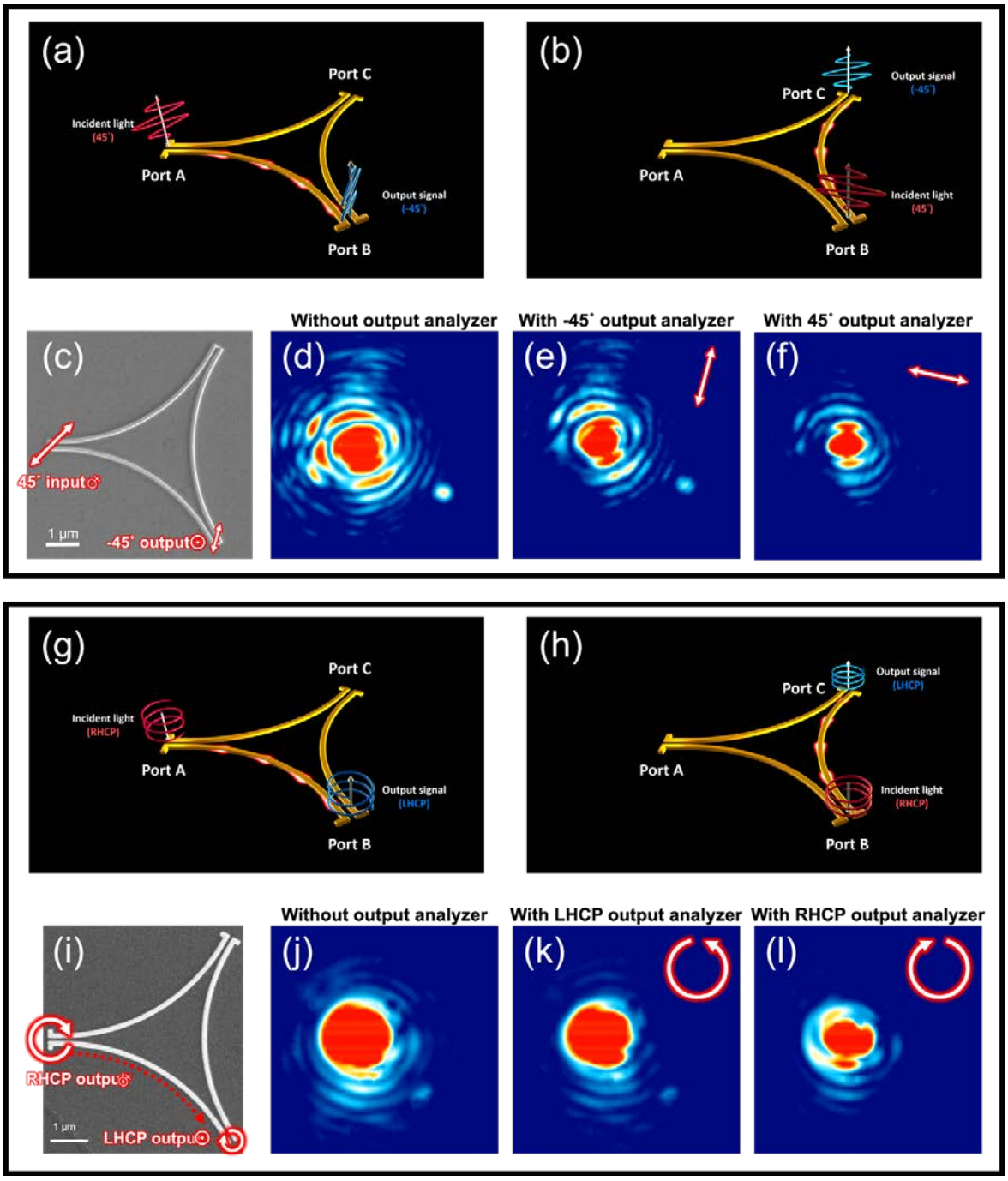

Figure S14. Schematic for operation of the circulator under linear polarization when (a) port A is excited using 45 degrees polarized light and (b) port B is excited using 45 degrees polarized light. SEM micrograph for the circulator with marked input and output polarization for conceptual clarity is shown in (c). Experimental images (d) in absence of, (e) with -45 degrees and (f) with 45 degrees output polarization analyzer. Schematic for operation of the circulator under circular polarization when (g) port A is excited using RHCP light and (h) port B is excited using RHCP light. SEM micrograph for the circulator with marked input and output polarization for conceptual clarity is shown in (i). Experimental images (j) in absence of, (k) with LHCP and (l) with RHCP output polarization analyzer.

The experimental images for the polarization analysis of the output signal when the circulator is excited at port A by 45 degrees polarized light as depicted for SEM micrographs shown in Figure S14(c) are shown in Figure S14(d) without a polarization analyzer between the CCD camera and the sample, (e) with -45 degrees polarization analyzer, and 45 degrees polarization analyzer (f). When the circulator is excited using RHCP light at port A as can be seen in Figure S14(g), the SPPs propagate through the single wire connecting port A to port B. The SPPs are thereafter scattered to the far field from port B changing the polarization to LHCP for the output light. Figure S14 (h) shows the functioning of the circulator when port B is excited by RHCP light. The experimental images for the polarization analysis of the output signal when the circulator is excited at port A by RHCP light as depicted for SEM micrographs shown in Figure S14(i) is shown in Figure S14(j) without a polarization analyzer between the CCD camera and the sample, (k) with LHCP polarization analyzer, and RHCP polarization analyser (l). The experimental results confirm the polarization conversion of the excitation beam.

6. Operational bandwidth

The operational bandwidth is defined as the wavelength range for which the device effectively acts as a functional circulator. Although, in FDTD calculations we observed very high crosstalk i.e. the ratio between the sum of powers from all undesired ports to the power from the desired output port. However, in experiments an Er-doped mode-locked fiber laser with 100 nm optical bandwidth centered at 1560 nm was used to excite the structure as seen in Figure S15. Therefore we experimentally observed the operational bandwidth to be 100 nm.

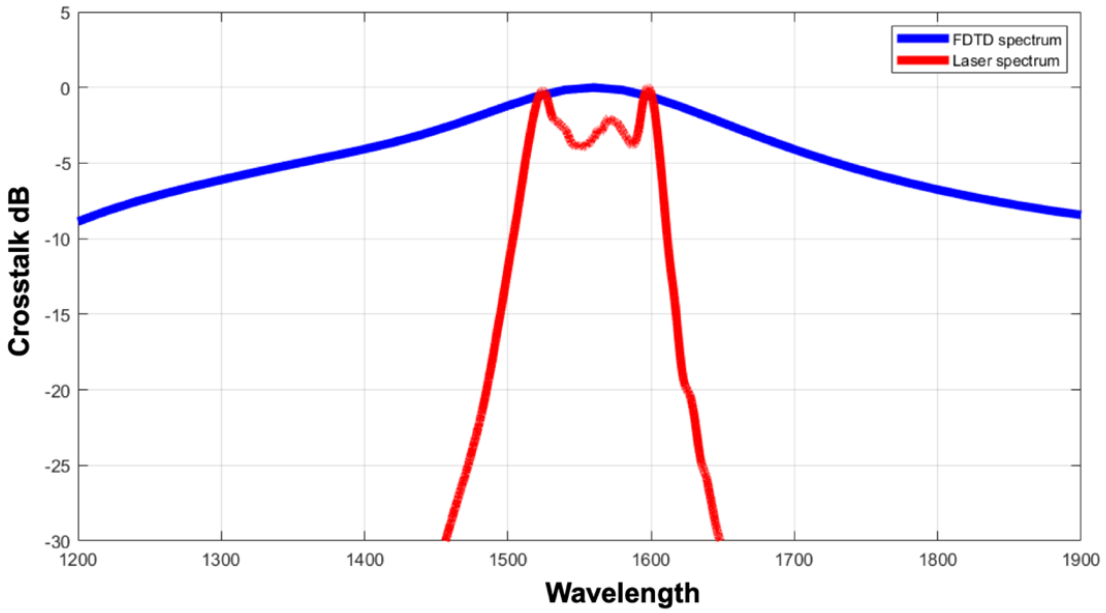

Figure S15. Wavelength versus crosstalk plot. Blue trace shows the FDTD calculations for the proposed structure whereas the red trace depicts the spectrum of the laser used in experiments for exciting the structure.